Design and Evaluation of Decision and Control Strategies for Autonomous Vision-based See and Avoid Systems

Aaron Mcfadyen[1] and Luis Mejias[2]

***Abstract*— This paper details the design and performance assessment of a unique collision avoidance decision and control strategy for autonomous vision-based See and Avoid systems. The general approach revolves around re-positioning a collision object in the image using image-based visual servoing, without estimating range or time to collision. The decision strategy thus involves determining where to move the collision object, to induce a safe avoidance manuever, and when to cease the avoidance behaviour. These tasks are accomplished by exploiting human navigation models, spiral motion properties, expected image feature uncertainty and the rules of the air. The result is a simple threshold based system that can be tuned and statistically evaluated by extending performance assessment techniques derived for alerting systems. Our results demonstrate how autonomous vision-only See and Avoid systems may be designed under realistic problem constraints, and then evaluated in a manner consistent to aviation expectations.**

I. Introduction

Unmanned Aircraft Systems (UAS) represent an important future technology, with the ability to augment or replace manned aircraft for a range of commercial applications [1]. As many industry sectors rapidly embrace the technology and further diversify the application base, there is an increased demand to allow unmanned aircraft regular access to unrestricted civilian airspace. Integrating unmanned aircraft into such a complex and structured environment is not trivial, and creates a set of challenging technical, regulatory and social issues that remain unresolved [2].

The most restrictive, and arguably most important issue is the lack of automated See and Avoid systems for unmanned aircraft [3]. This capability refers to the reactive short-term collision avoidance used by pilots in response to unplanned hazards such as terrain, conflicting aircraft or weather. It is an uncooperative approach primarily relying on the pilots' visual system, human collision avoidance behaviour, recollection of regulatory procedures and experience [4], [5]. Automating such a unique collision avoidance process and demonstrating an equivalent performance level to that of manned aircraft, presents a set of difficult problems [6]. Challenges remain regarding the design of detection, decision and control algorithms, as well as the performance evaluation techniques used to assess their utility and safety.

Regarding system design, a natural choice for object detection and tracking is the use of passive electro-optic devices [7]. They offer a lightweight, low-cost sensing solution for a range of unmanned aircraft regardless of size, weight and power limitations. A major drawback however is the limited amount of state information that can be reliably estimated. As distant aircraft appear as small, low-contrast slow moving point features in the image until seconds before collision (see Fig. 1), only relative angular measurements can be reliably obtained [8], [9]. Estimating relative position and velocity is considerably more complex for a number of reasons. The limited avoidance time available, unknown object motion (and size) and large relative geometries (scale) create significant observability issues that can cause difficulties for techniques leveraging passive ranging [10], visual looming [11], [12] or stereo vision [13]. Without relative position and velocity, determining safe avoidance maneuvers is then significantly challenging. The decision process is further complicated when considering that predictability is important for other airspace users. Automating the process then requires balancing expectations on sensor limitations with aviation procedures [14]. To this end, the following contributions are proposed in this paper:

Fig. 1. Example image taken from an unmanned aircraft (□) in a near-miss encounter with a Cessna 172R, where $r \approx 1500$m and $t_{\text{cpa}} \approx 15s$.

- A detailed analysis of a collision avoidance and resolution decision strategy that explicitly considers a realistic operational environment, visual sensing limitations and existing aviation procedures (rules of the air).
- Introduction of a novel system tuning and performance evaluation technique for autonomous vision-based See and Avoid decision strategies.
- First known attempt at statistically evaluating decision strategies explicitly designed for automated vision-based See and Avoid systems.

This paper is structured as follows. Section II provides a literature review of collision avoidance decision strategies and evaluation techniques in the context of See and Avoid. Section III describes the proposed collision avoidance strategy with emphasis on the decision aspects. The statistical performance evaluation method is then presented in Section IV, and used to assess the proposed decision strategy. Conclusions and further work are offered in Section V.

[1,2] are with the Science & Engineering Faculty, Queensland University of Technology, Brisbane, Australia. aaron.mcfadyen@qut.edu.au

II. Background

A. Decision Strategies

An automated collision avoidance decision strategy refers to the way in which the available state information is used to make choices aimed at resolving conflict. It involves deciding how to avoid the object (avoidance decision), implementing any prescribed action, and then deciding when to cease the avoidance behaviour (resolution decision). For vision-based See and Avoid systems, only relative state information obtained from imaging sensors can be used for each process.

If accurate relative position and velocity estimates could be acquired from image sequences, a large number of existing decision strategies used in robotics [15] and aviation could be considered [16]. These include approaches leveraging conflict probability (risk) estimates [17], dynamic programming and markov decision processes (MDP) [18], path planning [19], potential fields [20], and geometric optimisation such as collision cones and velocity obstacles [21]. Many of these can guarantee collision avoidance in the nominal case, with some approaches facilitating the simultaneous optimisation of multiple objectives such as miss distance, course deviation [22] and observability [23]. Although appealing, applying such strategies requires some rather optimistic or incorrect assumptions regarding the object behaviour and attributes, operational environment or sensor technology.

Assuming that only visual cues such as image position, velocity, shape and size can be reliably estimated from image sequences, then designing decision strategies is more restrictive. One approach is to formulate the problem in an image-based visual control framework, allowing the direct use of visual cues for decision and control. Such approaches better resemble See and Avoid behaviour, with many designs often inspired by insect and human navigation models.

Insects express a variety of different navigation behaviours. During the day, insects avoid collisions by assessing the optic flow field patterns created by nearby objects. The concept has been successfully applied to unmanned aircraft for large static collision objects [24], [25]. Decisions are qualitative in the sense that a scaled direction command is issued, without a specific aiming (reference) image point [26]. During the night, insects navigate by fixating the moons light rays at a constant position in the eye, which causes them to inadvertently avoid or collide with point light sources via a spiral trajectory [27]. This concept has been used implicitly [28], [29] and explicitly [30], [31] for avoidance of variable sized static objects. Dynamic objects were then considered for a subset of encounter types [32], [33]. Decisions are quantitative in the sense that a specific aiming (reference) image point is selected.

Humans tend to rely on relative angular observations when making avoidance decisions. Collisions are identified by a zero angular rate or a fixed angular position [34]. Collision avoidance is then achieved by adopting an anticipatory or predictive avoidance approach that forces a non-zero angular rate [35]. Decisions are again qualitative (up, right, speed up etc.) but can be influenced by prior knowledge [36]. For example, the decision to pass in front or below may be guided by experience [37], [38], or specific right-of-way rules such as those used at sea or in aviation [39]. Directly using angular rate to discriminate between See and Avoid encounters in a binary classification scheme has been investigated with varied results [18], [40]. Although effective at avoiding collisions, many non-collision encounters were incorrectly classified leading to unnecessary avoidance action [18]. This is likely due to the uncertainty on the visual observations. One way to remodel this approach is to assume an action will always be taken, whereby the specific action depends on the certainty or confidence in the visual observations. This means precautionary avoidance actions may then be adopted, which has also been observed in human See and Avoid behaviour [36], [37].

B. System Performance Evaluation

Performance evaluation for automated collision avoidance solutions generally refers to the process used to measure the utility and safety of the system. In the context of vision-based See and Avoid systems, this involves assessing the detection, decision and control system components individually and collectively. To ensure strict safety standards are maintained, performance evaluation methods should attempt to align with existing aviation processes. This means each system component may require rigorous testing in simulation and the intended operating environment, in an attempt to provide a comprehensive statistical performance analysis. Given the relative immaturity and diversity of proposed vision-based See and Avoid systems, a unified performance evaluation framework does not yet exist.

For detection systems, it is common to use principles from signal detection theory such as Receiver Operating Curves [41] to simultaneously visualise trade-offs in performance and design parameter selection. This allows system parameters, such as threshold placement, to be tuned in simulation and refined empirically via analysis of false alarm and correct detection statistics [42]. Other metrics such as the initial detection distance can be included, but are generally less useful when considering detection consistency [43].

For decision and control, performance is often assessed through stability guarantees, practical demonstrations (often on scaled down platforms) or in simulation studies. Metrics such as miss distance are commonly used, and trials are often restricted to a subset of encounters or under nominal operating conditions. Although useful, a statistical performance evaluation approach would offer a more complete assessment. As most decision strategies require parameter tuning, it would then make sense to use similar performance evaluation techniques to that used for detection. An attempt was made for alerting systems and then used to successfully evaluate existing aircraft collision avoidance systems (TCAS) [44]. Unfortunately, the approach cannot be applied directly to completely autonomous systems, vision-based or otherwise, so would require adaptation. If modified, such a framework would be useful for analysing and designing decision strategies solely based on assessing image feature

behaviour. The approach may also help to evaluate human navigation models and pilot See and Avoid behaviour. In this work, we combine the above findings and propose:

- A collision avoidance decision strategy based on assessing visual cues to re-position the object on the image surface using image-based visual control. Reference image positions are selected using the properties of spiral motion, aviation right-of-way rules and the expected uncertainty on image feature estimates.
- An initial investigation into a statistical performance evaluation approach for vision-based See and Avoid systems, by extending existing techniques for alerting systems to fully autonomous system. The approach is then used to optimise the proposed decision strategy, visualise performance and identify difficult collision encounter types.

III. Collision Avoidance & Resolution

A. Avoidance Maneuvers

Conical spiral trajectories are used as the basis for collision avoidance maneuvers. They describe the set of trajectories that circumscribe the surface of a cone, and are parametrised by a fixed velocity v and constant elevation $\beta \in \{0, \pi\}$ and bearing $\alpha \in \{-\pi, \pi\}$ angle to the apex [27]. Depending on the reference conical angles $\mathbf{c}^*(\beta^*, \alpha^*)$, divergent or convergent spirals (planar, ascending or descending) can be followed, with circular motion as a special case. Previous work has shown conical spirals to be a useful avoidance manuever for static objects, provided

$$|\alpha^*| \geq \pi/2, \qquad \beta^* \neq \pi/2 \tag{1}$$

The result is circular or divergent motion about the apex. In the notion of reducing course deviation, circular motion is then preferred [30], [31]. Collision avoidance of constant velocity objects is also possible by attempting to establish and track a conical spiral such that $\alpha^* = \pm\pi/2$ and $\beta^* \neq \pi/2$ [33]. Even if the reference spiral cannot be achieved for faster objects, attempting to establish and maintain it can result in safe avoidance behaviour. As evidence, consider an object moving with constant velocity v_t and constant heading in the xy-plane. An aircraft with velocity $v = 1$m/s then attempts to follow a reference spiral such that $\mathbf{c}^*(\pi/2, -\pi/2)$. Consider two cases in which the object moves with $v_t > v$ and $v_t < v$. For each case, the object adopts an initial relative heading $\bar{\alpha}_0 \in \{0, \pi/4, \pi/2, 3\pi/4, \pi, 5\pi/2, 3\pi/2, 7\pi/4\}$ and the aircraft is initially re-positioned to ensure $\alpha = -\pi/2$. The resulting aircraft trajectories are shown with respect to the object frame in Fig. 2.

For $v_t < v$ the aircraft tracks the reference conical angles, resulting in distorted spiral trajectory. For $\pi/2 \leq \bar{\alpha}_0 \leq 3\pi/2$ (*black, grey*), the aircraft initially moves away from the object following a safe avoidance maneuver. It is not until the aircraft attempts to overtake and pass in front of the object that a potential collision may occur. For $\bar{\alpha}_0 < \pi/2$ or $\bar{\alpha}_0 > 3\pi/2$ (*red*) the aircraft initially moves toward the object, such that an unsafe avoidance maneuver is adopted.

For $v_t > v$ the aircraft cannot track the reference conical angles for all object headings, and no spiral trajectory is

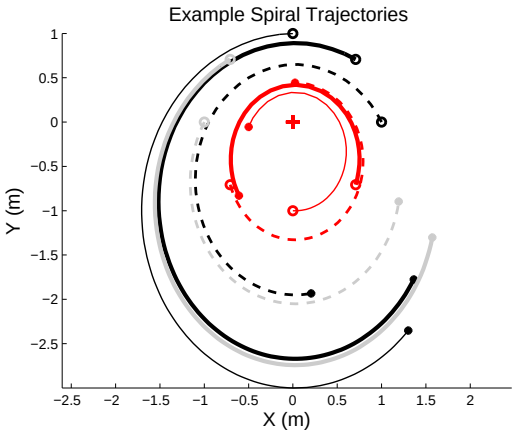

(a) $v_t < v = 0.5$m/s

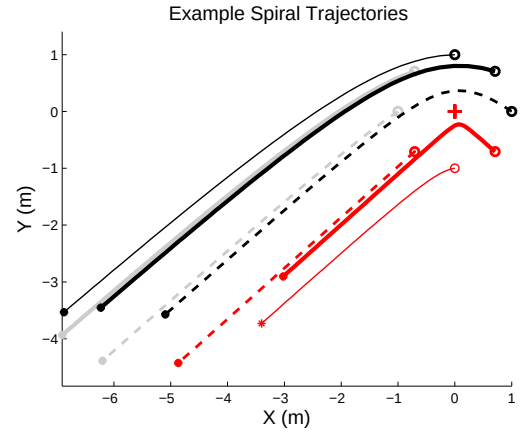

(b) $v_t > v = 1.5$m/s

Fig. 2. Example spiral trajectories displayed in the object frame $\mathcal{F}_o$ for a reference spiral $\mathbf{c}(\pi/2, -\pi/2)$. The initial object position in the world frame $\mathcal{F}_w$ is (1,1) and the aircraft is displaced by 1m (○,○,○). The object position (+) and safe (−/−) and unsafe (−) aircraft trajectories are shown.

adopted. However, for $\pi/2 \leq \bar{\alpha}_0 \leq 3\pi/2$, attempting to track the reference spiral initially moves the aircraft away from the object, as the correct avoidance direction is adopted. Again, for $\bar{\alpha}_0 < \pi/2$ or $\bar{\alpha}_0 > 3\pi/2$, the aircraft initially moves toward the object by adopting an unsafe avoidance direction. Importantly, the faster object has greater influence on the encounter geometry than the slower object.

The above analysis demonstrates spiral trajectories as a viable collision avoidance trajectory, with the difficulty residing in the determination of the reference spiral orientation ($\alpha = \pm\pi/2$). With unknown heading, it is impossible to analytically determine the optimal spiral direction to adopt. However, an avoidance decision is still required to determine which exact spiral to track for an arbitrary encounter. This ambiguity is addressed in the following section.

Remarks: *Simply moving left or right can result in an appropriate avoidance action, but it does not provide the same desirable qualities offered by attempting to follow a spiral path. First, the conical angles can be identified from a single point feature in the image, and tracked using various image-based visual control schemes. Second, the curved spiral trajectories force the aircraft back toward the original heading after avoidance, minimising unnecessary action.*

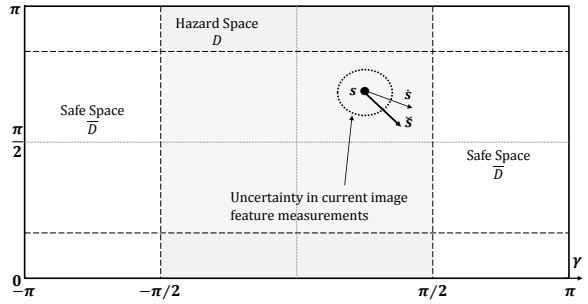

Fig. 3. Example planar representation of the spherical imaging surface, including an example object (•), bounded uncertainty ($\cdots$) on the image feature position ξ_s and danger area D (■).

B. Avoidance Decision

Consider a point image feature position $\mathbf{s}(\sigma, \gamma)$ and image feature rate $\dot{\mathbf{s}}(\dot{\sigma}, \dot{\gamma})$, where σ and γ denote de-rotated colatitude and azimuth angles measured from the image centre. Consider now a new metric $\breve{\mathbf{s}}$ derived from the image observations that can be used to represent the relative feature convergence, divergence or lack thereof such that

$$\breve{\mathbf{s}} = \mathrm{di}(\mathbf{s})\, \dot{\mathbf{s}}^T \tag{2}$$

where $\mathrm{di}(\cdot)$ denotes a diagonal matrix. A strongly diverging object moving away from the image centre will mean that $\breve{\mathbf{s}} \gg \mathbf{0}$. A strongly converging object moving toward the image centre will mean that $\breve{\mathbf{s}} \ll \mathbf{0}$. A relatively stationary object, that may exhibit some movement, means that $\breve{\mathbf{s}} \approx \mathbf{0}$.

Consider also some uncertainty vectors ξ_s and $\xi_{\dot{s}}$ for the image feature observations, whose elements consists of the variance ξ[1] on the image feature angular positions and rates such that $\xi_s = (\xi_\sigma \ \xi_\gamma)$ and $\xi_{\dot{s}} = (\xi_{\dot{\sigma}} \ \xi_{\dot{\gamma}})$. The variables can be used to denote uncertainty ellipses about the image features with respect to position and velocity such that

$$\mathbf{s}\, \mathrm{di}(\xi_s)\, \mathbf{s}^T = 0, \qquad \dot{\mathbf{s}}\, \mathrm{di}(\xi_{\dot{s}})\, \dot{\mathbf{s}}^T = 0 \tag{3}$$

In a similar fashion as above, consider an uncertainty threshold $\eta = (\eta_\sigma \ \eta_\gamma)^T$ such that

$$\eta = \mathrm{di}(\xi_{\mathbf{s}})\, \xi_{\dot{s}}^T \tag{4}$$

Now consider comparing the feature behaviour against a positive avoidance threshold at the initial confirmed detection instant t_d according to

$$\breve{\mathbf{s}}(t_d) \leqq \eta^T, \qquad \eta \geqq \mathbf{0} \tag{5}$$

The comparison evaluates the objects image behaviour whilst considering the expected measurement uncertainty. It helps qualitatively distinguish between the actual object behaviour and that induced by noise. To explain, consider the nominal case with perfect sensing and setting $\eta = \mathbf{0}$. Evaluating if $\breve{\mathbf{s}}(t_d) = \eta^T$ determines if a stationary object is in the centre of the image, or a dynamic object is indeed stationary in the image. These are the conditions known to lead to collision. For imperfect sensing, setting $\eta > \mathbf{0}$ and assessing if $\breve{\mathbf{s}}(t_d) \leqq \eta^T$ suggests the object is either relatively stationary in the image with arbitrary motion bounded by η^T, or very close to the image centre. In this case, the object may be considered a more significant collision threat than if $\breve{\mathbf{s}}(t_d) > \eta^T$. If the threshold is large such that $\eta \gg \mathbf{0}$, then almost all stationary, converging or diverging objects would be considered a major collision threat using the same assessment.

If the avoidance threshold is then used to denote the confidence (of variance) in the visual observations based on expected uncertainty, it represents a single parameter that can be tuned based on the degree of conservativeness that is desired. If large, the implication is that the camera is perhaps of lower quality or the ambient conditions are causing difficulties in object detection and tracking. If small, the opposite might be implied. Alternatively, the threshold value may be set based on the cameras measured performance during calibration, or updated during flight. The aforementioned variables are depicted in Fig. 3.

Once the object motion has been qualitatively assessed using the avoidance threshold, an appropriate reference image feature position $\mathbf{s}^*(\sigma^*, \gamma^*)$ is then selected. Provided that the image features are de-rotated in pitch and roll, the camera angles approximate the conical angles such that

$$\mathbf{s}^*(\sigma^*, \gamma^*) \approx \mathbf{c}^*(\beta^*, \alpha^*) \tag{6}$$

and so implicitly define a reference conical spiral [31]. Recall, determining the polarity of the reference image features (spiral direction), is impossible without knowledge of the object heading and velocity. Aviation flight rules, and in particular the right-of-way rules [39], [33], are therefore used as a convenient baseline solution to help resolve the ambiguity. The resulting logic for lateral and vertical avoidance are given by algorithm 1 and 2 (Appendix I). To help describe the algorithms, the avoidance decisions for some example cases shown in Fig. 4 and Fig. 5 are described below.

- ▷ *Example 1:* For $\breve{\sigma}_1 > \eta_\sigma$, the object is diverging in the top half plane. It is likely a non-crossing, non-collision object (either static or dynamic). The object is then allowed to pass above the aircraft by setting $\sigma^* = \pi/2 + \sigma_0$. For $\breve{\sigma}_2 > \eta_\sigma$, a similar situation occurs, but the object is now converging. The object is then allowed to cross in front of the aircraft by setting $\sigma^* = \pi/2 - \sigma_0$.
- ▷ *Example 2:* For $\breve{\sigma}_3 \leq \eta_\sigma$ and $\breve{\sigma}_4 \leq \eta_\sigma$, the objects are relatively stationary in the top half plane. They are likely collision objects (dynamic), but no right-of-way rules exist for the vertical dimension in non-overtaking encounters. The objects are forced to pass in front by setting $\sigma^* = \pi/2 \pm \sigma_0$ accordingly.
- ▷ *Example 3:* For $\breve{\gamma}_1$ and $\breve{\gamma}_2$, the object appears behind the aircraft and is not a collision object regardless of its behaviour. This is because it is no longer the primary responsibility of the aircraft. For $\breve{\gamma}_3 > \eta_\gamma$, the object is diverging in the right half plane. It is likely a non-crossing, non-collision object (either static or dynamic). The object is then allowed to pass to the right of the aircraft by setting $\gamma^* = \pi/2$. For $\breve{\gamma}_9 > \eta_\gamma$ the object is

[1]Although unconventional, the symbol ξ is used instead of σ^2 to denote variance to avoid confusion with the colatitude angle σ.

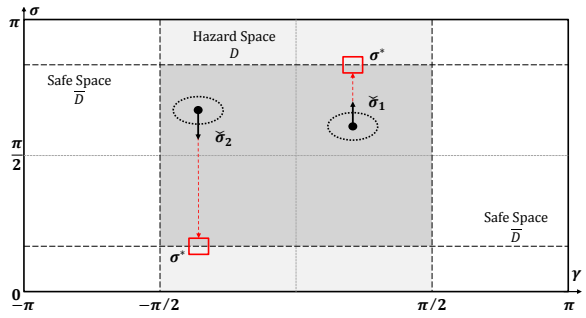

(a) Example 1

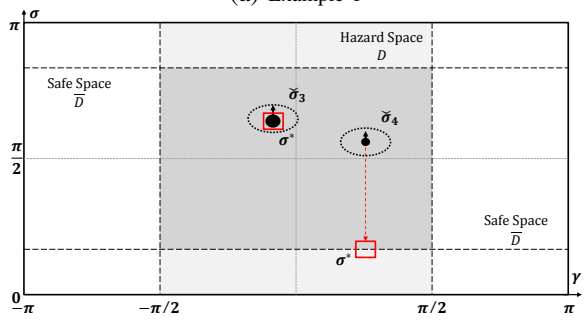

(b) Example 2

Fig. 4. Example collision avoidance cases. The image feature position (●) is shown, along with $\breve{\sigma}$ (⟶) and the resulting avoidance decision (or logic) outcome with respect to the colatitude reference σ^* (□).

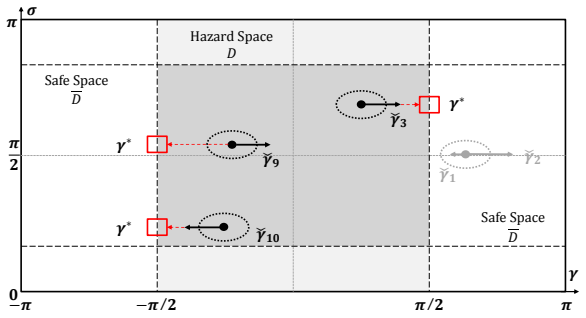

(a) Example 3

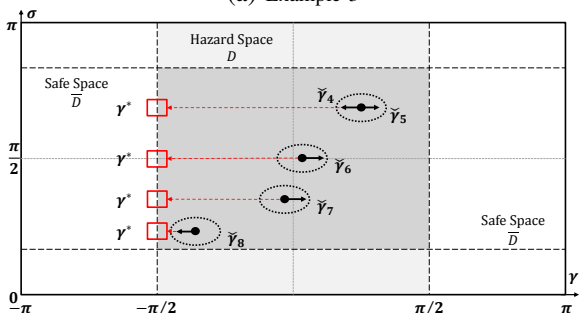

(b) Example 4

Fig. 5. Example collision avoidance cases. The image feature position (●) is shown, along with $\breve{\gamma}$ (⟶) and the resulting avoidance decision (or logic) outcome with respect to the reference azimuth angle γ^* (□).

converging in the left half plane. It is likely a crossing non-collision object (dynamic). For $\breve{\gamma}_{10} > \eta_\gamma$, the object is diverging in the left half plane. It is likely a non-crossing, non-collision object (either static or dynamic). In both cases however, applying the right-of-way rules means the object is required to pass behind the aircraft by setting $\gamma^* = -\pi/2$.

▷ *Example 4:* For $\breve{\gamma}_4 \leq \eta_\gamma$ and $\breve{\gamma}_5 \leq \eta_\gamma$, the object is relatively stationary in the right half plane. It is likely a crossing collision object (dynamic), and right-of-way must be given. The object is then allowed to pass in front by setting $\gamma^* = -\pi/2$. For $\breve{\gamma}_6 \leq \eta_\gamma$, the object may be static and directly in front of the aircraft, or dynamic and just prior to collision. This constitutes a near-head on encounter, so the aircraft must turn right. As such, the object is allowed to pass in front by setting $\gamma^* = -\pi/2$. For $\breve{\gamma}_7 \leq \eta_\gamma$ and $\breve{\gamma}_8 \leq \eta_\gamma$, the object is relatively stationary in the left half plane. It is likely a crossing collision object, and right-of-way must be given. In this case however, the aircraft has right-of-way which means the object is required to pass behind. As such, the object is forced to pass behind by setting $\gamma^* = -\pi/2$.

Remarks: *Action is always taken with decoupled lateral and vertical avoidance decisions resulting in a mixture of the above cases. Decisions are intended to be more predictable from a pilots' perspective instead of guaranteeing collision avoidance or geometric optimality. Additionally, if the object employs the same avoidance strategy, the resulting motion is complementary. For example, if the object observes the aircraft on the right, the object gives way and the aircraft has right-of-way such that $\gamma^* = -\pi/2$ for both platforms.*

C. Avoidance Control

Spherical image-based visual servoing is used to track the reference image features. As only a single point is observed, only two degrees of freedom can be directly controlled from the visual feedback. To remain applicable to all platforms (rotary and fixed wing), only vertical velocity (or position) and yaw rate (or roll angle) are visually controlled. The remaining degrees of freedom can be controlled separately using a series of PID and LQRI controllers to maintain a fixed forward speed. The result is a partitioned control approach in which the image-based control can be cast in a classical or predictive (optimal) control framework.

Using classical methods, the control vector $\mathbf{u}_z$ is found by assuming an exponential decrease in the image feature error $\mathbf{e}$ such that

$$\mathbf{u}_z(t) \quad = \quad \hat{\mathbf{L}}_z^{-1}\left(-\lambda\mathbf{e}(t) - \hat{\mathbf{L}}_{xy}\mathbf{v}_{xy}(t)\right) \tag{7}$$

where $\hat{\mathbf{L}}_z$ and $\hat{\mathbf{L}}_{xy}$ represent the z and xy axis components of the approximate spherical image Jacobian respectively. The $\mathbf{v}_{xy}$ term denotes the translational and rotational velocities about the x and y axis, and λ is a constant gain term. The image Jacobian is approximate in the sense that it is parametrised by a fixed reference range value. This is not restrictive as stable, conservative avoidance trajectories can be obtained by overestimating its value and assuming a moderate gain term [30].

Using predictive methods, an optimal control sequence $\mathbf{u}_z^*(\cdot)$ is found by minimizing a cost function J_s subject to control, platform and sensing (visibility) constraints such that

$$\mathbf{u}_z^*(\cdot) \quad = \quad \underset{\mathbb{U}}{\operatorname{argmin}}\ J_s(\mathbf{z}(t), \mathbf{u}_z(\cdot)) \tag{8}$$

where $\mathbb{U}$ defines the control constraint domain, and $\mathbf{z}$ denotes a mixed state consisting of both image features and vehicles states. The optimisation problem is solved over a finite time horizon using standard nonlinear model predictive control approaches. The approach offers greater flexibility than classical methods, allowing the explicit consideration of platform dynamics and associated constraints, whilst remaining aligned to anticipatory human navigation models. Stability-based designs for spiral motion also exist [31].

For both control approaches, an integral term can be added to the control at each iteration to help account for model mismatch and added uncertainty. For dynamic objects, this helps compensate for the generally unknown object motion. Using predictive control, the augmented control $\mathbf{u}_z^\star$ is then

$$\mathbf{u}_z^\star(t) \quad = \quad \mathbf{u}_z^*(t) + \lambda_i \int^w \mathbf{e}(t)\, dt \tag{9}$$

where λ_i is a fixed integral gain term and w denotes an arbitrary time window. These parameters should be selected in conjunction with the control constraint domain to ensure stable control. As control is not the focus of this work, we leverage past designs using the predictive approach outlined above, but include integral action (9). A detailed outline of the controller including all parameters, dynamic models and the image Jacobian structure can be found in [32].

D. Resolution Decision

A range independent heading-based criteria is used to indicate an appropriate time to stop the avoidance. As the platform avoids the object using a spiral path, it inadvertently attempts to return to its original heading upon initial avoidance action $\psi(t_d)$. Ceasing spiral motion when $\psi(t) = \psi(t_d)$ then stops the avoidance behaviour before the point of minimum separation, with the aircraft displaced from its original path and re-tracking its initial heading. The amount of time before the point of minimum separation depends on the maneuvering required to establish the spiral. This depends on the closing velocity, or difference between the reference azimuth and relative heading.

The larger the closing velocity, the less the aircraft maneuvers to establish the spiral and then return to its initial heading. This is because the object motion now reinforces the aircraft's attempt to establish the spiral. Once established, the aircraft must turn quickly to maintain the spiral, decreasing the time spent tracking the spiral before re-establishing the initial heading. So for a given relative velocity, the larger the difference between the reference azimuth and relative heading, the closer the stopping time is to the point of minimum separation. The effect is seen in Fig. 6(a) for $v_t < v$, where the closing velocity increases as the relative heading approaches a head on encounter ($\psi(t_d) = 3\pi/2$). The result is further amplified in Fig. 6(b) where $v_t > v$ and the stopping instance tends toward the time of minimum separation for all $\psi(t_d)$.

An effective resolution decision strategy can then be designed based solely on monitoring the platform heading. The simplest approach is stop the avoidance when $\psi(t) = \psi(t_d)$,

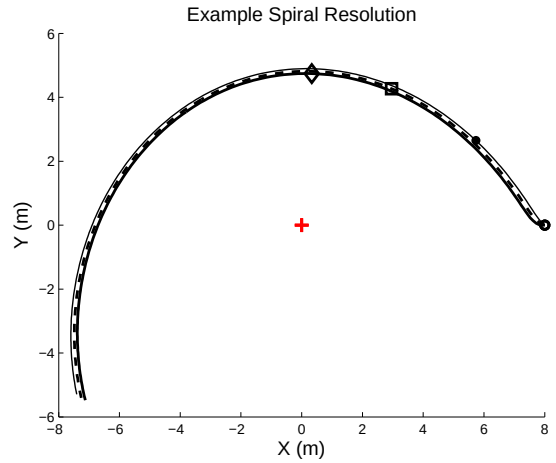

(a) $v_t < v$

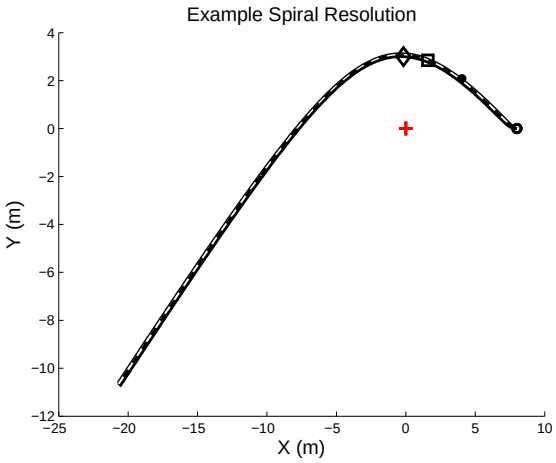

(b) $v_t > v$

Fig. 6. Example resolution cases displayed in the object frame $\mathcal{F}_o$ for a reference spiral $\mathbf{s}^* = \mathbf{c}^*(\pi/2, -\pi/2)$. The object initial position in the world frame is (1,1) and the aircraft is initial displaced by 1m (○,○). The aircraft position (–/––/–) and corresponding resolution instance (◇/□/●/) are given for $\psi(t_d) \in \{3\pi/2, 5\pi/3, 11\pi/6\}$ respectively.

but this assumes perfect state information so will fail in the presence of noise. If $|\psi(t_d + \delta t)| < |\psi(t_d)|$ due to turbulence or poor sensor quality, avoidance will be stopped prematurely resulting in a potentially unsafe situation [30]. A better approach is to wait until the reference image features are tracked, and then place a small positive threshold ϵ about the reference heading such that avoidance is stopped when

$$\psi(t_d) - \epsilon < \psi(t) < \psi(t_d) + \epsilon \tag{10}$$

Although coupled to the visual control, there is no way to measure the degree to which each competing objective is accomplished. To do this, a cost function J_ψ external to the visual control could be used to provide an explicit trade-off in obtained the reference spiral and stopping the avoidance. Thresholding the minimum value J_ψ^* could be considered a proxy to continuously assessing how well both objectives are satisfied. The resulting control $\mathbf{u}_z^{\star\star}$ can be expressed as,

$$\mathbf{u}_z^{\star\star}(t) = \begin{cases} \bar{\mathbf{u}}_z(t), & \forall\ J_\psi^*, \quad t < t_d \ \vee\ t_s \leq t < \infty \\ \mathbf{u}_z^\star(t), & J_\psi^* > \epsilon,\ t_d \leq t < t_s \end{cases} \tag{11}$$

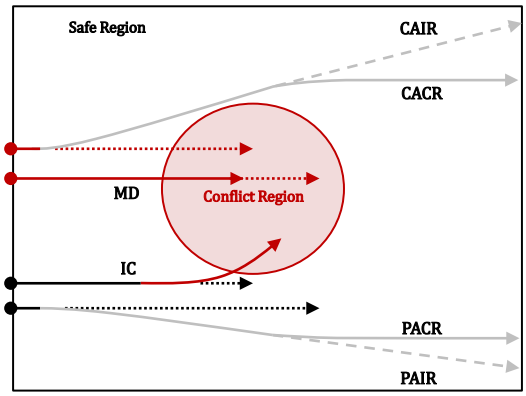

Fig. 7. Automated collision avoidance outcomes

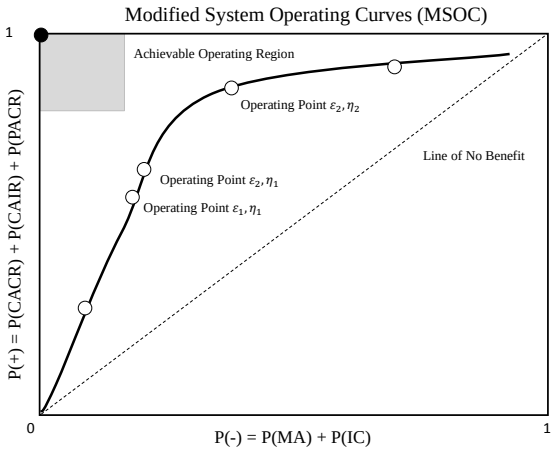

Fig. 8. Example Modified System Operating Curve

where $\bar{\mathbf{u}}_z$ denotes non-visual control. This is the approach taken in this paper, with details of the cost function used for resolution decisions provided in [33].

IV. System Evaluation

The evaluation technique extends existing probabilistic approaches used in alerting systems and signal detection theory. The framework offers a means to simultaneously asses system performance and optimise the parameters and thresholds (η, ϵ) used in the decision and control strategy. The framework requires the identification of an augmented set of collision outcomes, and the development of associated statistical performance metrics that can be visualised using derivatives of receiver or system operating curves.

A. Collision Avoidance Outcomes

The specific outcome of a potential collision encounter is a function of the relative geometry, minimum safety margins and the complex interactions between collision avoidance system parameters. It is then intractable to enumerate each unique outcome, so the resulting collision state is categorised according to a discrete set of outcomes types.

A simple binary classification consisting of collision or miss outcomes, does not provide sufficient granularity to account for the inclusion of the reactive fully automated collision avoidance system. The outcome categories need to consider that action is always taken, albeit different based on the avoidance decision, and that the action needs to be stopped. Just because an avoidance action was taken, does not ensure that the avoidance behaviour was stopped and the collision was resolved. The encounter outcome categories are therefore extended to include

PACR	:	Precautionary Avoidance & Correct Resolution
PAIR	:	Precautionary Avoidance & Incorrect Resolution
CACR	:	Correct Avoidance & Correct Resolution
CAIR	:	Correct Avoidance & Incorrect Resolution
MA	:	Missed Avoidance
IC	:	Induced Collision

where precautionary action is associated with non-collision encounters. **PACR** results when precautionary action is taken and then successfully stopped. **PAIR** results when precautionary action is taken but is incorrectly (or unsuccessfully) stopped. **CACR** results when collision avoidance action is required and taken, and then successfully resolved. **CAIR** results when collision avoidance action is required and taken, but then incorrectly resolved. **MA** results when a collision was present, but not avoided. **IC** results for non-collision encounters in which action induced a collision. For **MA** and **IC**, resolution outcomes do not make sense. The collision avoidance outcome categories are depicted in Fig. 7.

B. Modified System Operating Curves

A modified system operating curve is constructed using the observed counts of each outcome type for a large number of encounter scenarios under different system parameters. The plot consists of two axis, one denoting the probability of a desirable outcome $P(+)$ and the other the probability of an undesirable outcome $P(-)$ where

$$P(+) = P(\mathbf{CACR}) + P(\mathbf{CAIR}) + P(\mathbf{PACR}) \quad (12)$$

$$P(-) = P(\mathbf{MA}) + P(\mathbf{IC}) \quad (13)$$

Each individual probability or statistical performance metric is calculated over the total number of collision N and non-collision encounters M. For example,

$$P(\mathbf{CACR}) = \frac{\#\mathbf{CACR}}{N},\ P(\mathbf{PAIR}) = \frac{\#\mathbf{PAIR}}{M}, \quad \ldots \quad (14)$$

Of note, $P(\mathbf{CAIR})$ is considered desirable as the primary concern is to avoid collision. The undesirable outcome $P(\mathbf{PAIR})$ is excluded, but can be included if required.

For a given set of controller parameters, decision thresholds (η, ϵ) and noise characteristics, the above metrics (12)-(13) are determined and plotted as a single operating point. The system parameters are then altered and the metrics are re-evaluated to obtain a set of points, resulting in a curve. The goal being to move toward the fictitious ideal operating point in the upper left corner. At this point, no collisions occur and avoidance action is always stopped for both collision and non-collision encounters.

To isolate the decision strategy, the controller and noise parameters are fixed and only the avoidance and resolution

thresholds are varied. The effect of each decision threshold on system performance can then be visualised and subsequently optimised accordingly, as the thresholds are mutually exclusive and decoupled. An example of such a modified system operating curve is shown in Fig. 8.

C. Simulation Architecture

The avoidance decision, avoidance control and resolution decision strategies are combined in a simulation architecture developed in MATLAB, and using external optimisation routines [45]. A small quadrotor platform is assumed, whereby a simplified point mass dynamic model is used for the predictive controller and a realistic empirically derived dynamic model [32] is implemented during simulation. The linearised object motion model expresses itself only as a point image feature. The controller frequency f_c is faster than the image processing rate f_i, with objects detected within the range r_0. Additive uncertainty includes sensor (image feature) noise $q_s(t)$, imperfect actuation $q_c(t)$, turbulence $w_g(t)$ and ambient wind $w_a(t)$ (Appendix II).

The avoidance threshold was initially set such that $\eta = (\xi_\sigma \;\; \xi_\gamma)$, and then varied using a scaling factor $\lambda_\eta \in \{1/8, 1/4, 1/2, 1, 2, 4, 8\}$. Avoidance thresholds significantly below and above the expected image feature uncertainty where thus evaluated. The resolution threshold was set such that $\epsilon \in \{0.02, 0.05, 0.07, 0.09, 0.15, 0.30\}$. The values are coupled to the weighting matrix scales used in the cost function J_ψ, and represent liberal ($\epsilon \approx 0.30$) and conservative ($\epsilon \approx 0$) values. For each η and ϵ, 1000 constant velocity collision and 1000 non-collision encounters were simulated in a scaled-down See and Avoid environment (1:100). Given the control constraints, nominal collision boundary $r_c = 0.25$m and initial geometry, no encounters were considered whereby avoidance would be infeasible for any controller.

D. Results

Fixing the avoidance threshold ($\lambda_\eta = 1$), the resolution performance was first evaluated. System performance was acceptable, and was significantly influenced by the resolution threshold value. The operating points move toward the ideal operating point as the threshold increases, before diverging when the threshold is increased such that $\epsilon > 0.15$. The result articulates the tradeoff between maintaining the reference spiral and ceasing avoidance behaviour. For small thresholds, resolution is conservative as it becomes difficult to meet the threshold value ($J_\psi > \epsilon, \; \forall\, t$). The platform is reluctant to leave the spiral path, further encircling the object and providing the opportunity to induce future collisions ($P(+) \approx 70\%$, $P(-) \approx 2\%$). As the threshold is increased such that $\epsilon > 0.15$, resolution becomes very liberal as it becomes easier to meet the threshold value. Avoidance action may be stopped at an earlier instance ($J_\psi < \epsilon, \; t \approx t_d$), so the aircraft may not have maneuvered enough to avoid a collision. The amount of correct resolutions increases at the expense of increased collision risk, moving the curve rightwards away from the ideal operating point ($P(+) \approx 90\%$, $P(-) \approx 5\%$).

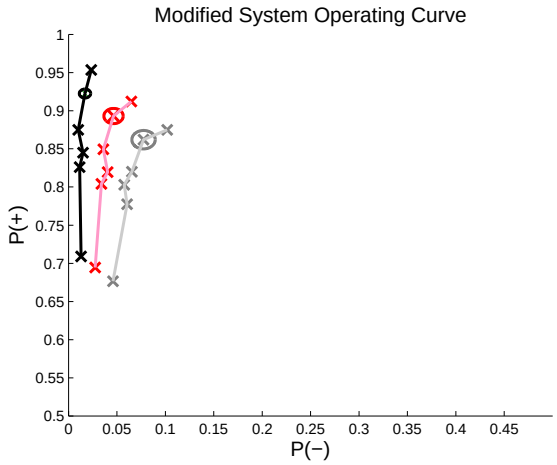

Fig. 9. Example modified system operating curve for variable $\epsilon \in (0.02, 0.30)$ (×) and $\lambda_\eta \in (1/8, 8)$ values. The set of avoidance thresholds for $\epsilon = 0.15$ is approximated using the region Ω_η (○/○/○). Three curves are shown for a collision boundary r_c of 0.125 (−), 0.25 (−) and 0.5 (−).

Fixing the resolution threshold ($\epsilon = 0.15$), the avoidance performance was then evaluated. System performance was surprisingly good ($P(+) \approx 87 - 91\%$, $P(-) \approx 2\%$), and less influenced by the avoidance threshold value. The operating point locations lack a distinguishable pattern with respect to changes in η, residing in a small region about the nominal point $\bar{\eta}$ for $\lambda_\eta = 1$. For example, $\lambda_\eta = 4$ shows improved performance, but $\lambda_\eta = 8$ shows degraded performance compared to $\lambda_\eta = 2$. An operating region Ω_η may then be coarsely approximated by finding the maximum 2-norm distance d_η between the nominal operating point and $\eta \in (\bar{\eta}/8, 8\bar{\eta})$. A circular region of radius d_η can then be used to approximate the region.

The above result can be interpreted two ways. Either there is insufficient simulations to draw adequate conclusions, or there exists encounter geometries that cause problems for the avoidance approach regardless of the threshold value. The latter may be due to the reliance on right-of-way rules or difficulties in distinguishing collision and non-collision objects under image feature uncertainty. By always acting however, performance surpasses that of similar systems using angular measurements to only avoid collision objects [10]. In such systems, both positive and negative outcomes were high ($P(+) \approx P(-) \approx 90\%$).

Combining the above outcomes, the resulting modified system operating curves for variable collision boundaries are shown in Fig. 9. Selecting a smaller collision boundary improves performance, but the results are open to interpretation subject to aircraft size. For example, the results suggest that for $r_c = 0.125$ the system can be 95% effective at avoiding collisions between two small aircraft with radius ≤ 0.0625m with zero separation. Conversely, for $r_c = 0.5$ the system can be only 85% effective at avoiding collisions involving these same aircraft, but with non-zero separation instead.

As a final result, the performance evaluation strategy can help identify the collision geometries which cause the decision strategy to fail. This is done by re-simulating the object trajectories in the aircraft reference frame for all collision

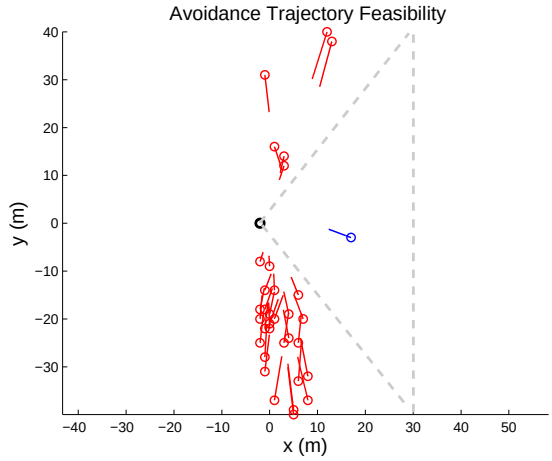

Fig. 10. Example illustration of all collision trajectories for an encounters set of 2000. Object initial position (○/○) and trajectories for missed avoidance (−) and induced collisions (−) are shown up to the time of collision. The aircraft initial position (○) without avoidance trajectory is also shown.

encounters (missed avoidance and induced collisions), up until the time of minimum separation. This is depicted in Fig. 10 for $\epsilon = 0.15$, $\lambda_\eta = 1$ and $r_c = 0.125$. The results show that the decision strategy handles head-on encounters very well, with only a single induced collision and no missed avoidances. Crossing collision encounters are more difficult to manage, with object trajectories originating near ± 90 degrees causing the most difficulty. Similar results are also obtained for different decision thresholds and collision boundaries, which provides some valuable insight into the effectiveness of the right-of-way rules themselves.

Remarks: *The results omit the probability of a collision encounter itself. If included, system performance would appear to improve given the rarity of the event. Instead, the probability of an encounter is unity with collisions and non-collisions equally likely to avoid misleading the results.*

V. Conclusions

Design and certification of See and Avoid systems is a challenging task that remains in the developmental stage. The approach presented in this paper demonstrates how an effective vision-based decision and control strategy for automated See and Avoid systems can be designed, tuned and statistically evaluated in a generalised framework. Initial results suggest the proposed strategy is over 90% effective at avoiding collisions, with only a 2-5% chance of a negative outcome. Additionally, the approach could be used to augment existing collision avoidance approaches.

This work constitutes a particularly unique contribution toward the progression of automated See and Avoid systems, and provides a good foundation in which to stem further research and development. This may include augmenting the performance evaluation approach to account for detection performance metrics and the likelihood of specific encounter types (collision, non-collision, near miss etc.).

Acknowledgements

This work was supported by the Institute for Future Environments (IFE) and the Australian Research Centre of Aerospace Automation (ARCAA) at Queensland University of Technology, Brisbane, Australia.

Appendix I

Algorithm 1 Avoidance Decision Strategy - Azimuth

if $\gamma \in D$ **then** ▷ Danger Area
  if $\breve{\gamma} < \eta_\gamma$ **then** ▷ Convergent, Centreline or Static Features
    $\gamma^* = -\pi/2$ ▷ **Allow Crossing
    Right-of-Way Rules, CAR 162(1-4)
  else ▷ Divergent Features
    if $\gamma < 0$ **then** ▷ Left Centreline
      $\gamma^* = -\pi/2$ ▷ **No Crossing
    else ▷ Right Centreline
      $\gamma^* = \pi/2$ ▷ **No Crossing
    end if
  end if ▷ Static or Centerline Features
else ▷ Outside Danger Area
  $\gamma^* = \gamma$ ▷ **No Movement
end if ** ***Aircraft Action***

Algorithm 2 Avoidance Decision Strategy - Colatitude

Set $\sigma = \sigma - \pi/2^\dagger$, $\sigma_o^* = 35\pi/180^\ddagger$
if Object Above Horizontal **then**
  if $\breve{\sigma} > \eta_\sigma$ **then** ▷ Divergent Features
    $\sigma^* = \pi/2 + \sigma_o^*$ ▷ **No Crossing
  else if $\breve{\sigma} < -\eta_\sigma$ **then** ▷ Convergent Features
    $\sigma^* = \pi/2 - \sigma_o^*$ ▷ **Allow Crossing
  else ▷ Static or Centerline Features
    if Overtaking **then** ▷ Overtaking
      $\sigma^* = \sigma$ ▷ **No Movement, ***CAR 162(4)***
    else Not Overtaking
      $\sigma^* = \pi/2 - \sigma_o^*$ ▷ **Allow Crossing
    end if
  end if
else Below Above Horizontal
  Reciprocal Logic
end if ** ***Aircraft Action***

$^\ddagger\sigma_0$ is located in a relatively nonlinear region of the image surface to improve control performance regarding stability and feasibility [31].

Appendix II

Simulation & Control Parameters

Parameter	Value	Units
f_c	40	Hz
f_i	10	Hz
ξ_s	(0.04, 0.04)	rad
$\xi_{\dot{s}}$	(0.04, 0.04)	rad/s
t_{cpa}	[5 55])	s
r_0	[0 40]	m
v_t	$[-0.5\ 0.5]$	m/s
$w_g(t)$	$\mathcal{N}(\mathbf{0}_3, \mathbf{I}_3)$	rad/s
$w_a(t)$	$\mathcal{N}(\mathbf{0}_3, 0.25\mathbf{I}_3)$	m/s
$q_c(t)$	$\mathcal{N}(\mathbf{0}_2, 0.02\mathbf{I}_2)$	rad
$q_s(t)$	$\mathcal{N}(\mathbf{0}_2, \xi_s\mathbf{I}_2)$	N, rad/s
v	0.1	m/s
λ_i	0.01	-
w	$10/f$	s

REFERENCES

[1] K. Valavanis, "Unmanned aircraft systems: the current state-of-the-art," *Springer*, 2013

[2] K. Dalamagkidis, K. Valavanis, and L. Piegl, "On unmanned aircraft systems issues, challenges and operational restrictions preventing integration into the national airspace system," *Progress in Aerospace Sciences*, vol. 44, no. 7-8, pp. 503-519, Oct-Nov. 2008

[3] P. Angelov, "Sense and avoid in UAS: research and application," *John Wiley & Sons*, 2012

[4] Australian Transport Safety Bureau (ATSB), "Limitations of the see-and-avoid principle," *Tech. Report*, Canberra, Australia, Nov. 2004

[5] C. Morris "Midair collisions: limitations of the see-and-avoid concept in civil aviation," *Aviation, Space, and Environmental Medicine*, vol. 76, no. 4, pp. 357-365, April 2005

[6] X. Prats, L. Delgado, J. Ramírez, P. Royo and E. Pastor, "Requirements, issues, and challenges for sense and avoid in unmanned aircraft systems," *Journal or Aircraft*, vol. 49, no. 3, pp. 677-687, May 2012

[7] J. Lai J. Ford L. Mejias and P. O'Shea, "Characterization of sky-region morphological-temporal airborne collision detection," *Journal of Field Robotics*, pp. 171-193, vol. 30, no. 2, March-April 2013

[8] J. Lai, J. Ford, L. Mejias, and P. O'Shea, "Vision-based estimation of airborne target pseudobearing rate using hidden Markov model filters," *IEEE Trans. Aerospace and Electronic Systems*, vol. 49, no. 4, pp. 2129-2145, Oct. 2013

[9] G. Fasano, D. Accardo, A. Tirri and A. Moccia, "Morphological filtering and target tracking for vision-based UAS sense and avoid," *IEEE Int. Conf. Unmanned Aircraft Systems (ICUAS'14)*, pp. 430-440, May 2014

[10] O. Shakernia, M. Chen, and V. Raska, "Passive ranging for uav sense and avoid applications," *AIAA Infotech@Aerospace Conf. and Exhibit*, pp. 1-10, March 2005

[11] T. Molloy, J. Ford and L. Mejias, "Looming aircraft threats : shape-based passive ranging of aircraft from monocular vision," *Australian Conf. Robotics and Automation*, Dec. 2014

[12] H. Choi, Y. Kim and I. Hwang "Reactive collision avoidance of unmanned aerial vehicles using a single vision sensor," *Journal Guidance, Control and Dynamics*, vol. 36, no. 4, pp. 1234-1240, 2013

[13] S. Hrabar, "An evaluation of stereo and laserbased range sensing for rotorcraft unmanned aerial vehicle obstacle avoidance," *Journal of Field Robotics*, vol. 29, no. 2, pp. 215-239, 2012

[14] A. Mcfadyen and L. Mejias, "A survey of autonomous vision-based see and avoid for unmanned aircraft systems," *Progress Aerospace Science*, 2015 *(submitted)*

[15] M. Hoy, A. Matveev and A. Savkin, "Algorithms for collision-free navigation of mobile robots in complex cluttered environments: a survey," *Robotica*, pp. 1-35, March 2014

[16] J. Kuchar and L. Yang, "A review of conflict detection and resolution modeling methods," *IEEE Trans. Intelligent Transportation Systems*, vol. 1, no. 4, pp. 179-189, Dec. 2000

[17] B. Vanek, T. Péni, P. Bauer, and J. Bokor, "Vision only sense and avoid: a probabilistic approach," *American Control Conference (ACC'14)*,1204-1209, 2014

[18] M Kochenderfer, J. Griffith, and J. Kuchar, "Hazard alerting using line-of-sight rate," *AIAA Guidance, Navigation and Control Conference and Exhibit*, 18-21 August, 2008

[19] J. Cobano, R. Conde, D. Alejo and A. Ollero, "Path planning based on genetic algorithms and the monte-carlo method to avoid aerial vehicle collisions under uncertainties," *IEEE Int. Conf. Robotics and Automation (ICRA'11)*, pp. 4429-4434, May 2011

[20] J. Ruchti, R. Senkbeil, J. Carroll, J. Dickinson, J. Holt and S. Biaz, "Unmanned aerial system collision avoidance using artificial potential fields," *Journal of Aerospace Information Systems* vol. 11, no. 3 pp. 140-144, 2014

[21] A. Alexopoulos, A. Kandil, P. Orzechowski and E. Badreddin, "A comparative study of collision avoidance techniques for unmanned aerial vehicles," *IEEE Int. Conf. Systems, Man, and Cybernetics (SMC'13)*, pp. 1969-1974, Oct. 2013

[22] P. Zapotezny-Anderson and J. Ford, "Optimal-stopping control for airborne collision avoidance and return-to-course Flight," *Australian Control Conference (AUCC'11)*, pp. 155-160, Nov. 2011

[23] H. Yu, R. Sharma, R. Beard and C. Taylor, "Observability-based local path planning and obstacle avoidance using bearing-only measurements," *Robotics and Autonomous Systems*, vol 61, no. 12, pp. 1392-1405, Dec. 2013

[24] W. Green and P. Oh, "Optic-flow-based collision avoidance," *IEEE Robotics & Automation Magazine*, vol. 15, no. 1, pp. 96-103, March 2008

[25] C. Bills, J. Chen and A. Saxena, "Autonomous MAV flight in indoor environments using single image perspective cues," *IEEE Int. Conf. Robotics and automation (ICRA'11)*, pp. 5776-5783, May 2011

[26] A. Beyeler, J. Zufferey and D. Floreano, "Vision-based control of near-obstacle flight," *Autonomous Robots*, vol. 27, no. 3 pp. 201-219, 2009

[27] K. Boyadzhiev, "Spiral and conchospirals in the flight of insects," *The college Mathematics Journal*, vol. 30, no. 1, pp. 22-31, Jan. 1999

[28] J. Saunders, R. Beard, and J. Byrne, "Vision-based reactive multiple obstacle avoidance for micro air vehicles," *American Control Conference (ACC'09)*, pp. 5253-5258, June 2009

[29] X. Yang, L. Mejias, and T. Bruggemann, "A 3D collision avoidance strategy for uavs in an non-cooperative environment," *Journal of Intelligent Robotic Systems*, vol. 70, no. 1-4, pp. 315-327, April 2013

[30] A. Mcfadyen P. Corke and L. Mejias, "Rotorcraft collision avoidance using spherical image-based visual servoing and single point features," *IEEE/RSJ Int. Conf. Robotics and Intelligent Systems (IROS'12)*, pp. 1199-1205 , Oct. 2012.

[31] A. Mcfadyen, P. Corke and L. Mejias, "Visual predictive control of spiral motion," *IEEE Trans. Robotics*, vol. 30, no. 6, pp. 1441-1454, 2014

[32] A. Mcfadyen L. Mejias P. Corke and C. Pradalier, "Aircraft collision avoidance using spherical visual predictive control and single point features," *IEEE/RSJ Int. Conf. Robotics and Intelligent Systems (IROS'13)*, pp. 50-56, Nov. 2013

[33] A. Mcfadyen, A. Durand-Petiteville and L. Mejias, "Decision strategies for automated visual collision avoidance," *Proc. Int. Conf. Unmanned Aircraft Systems (ICUAS'14)*, pp. 715-725, May 2014

[34] B. Fajen and W. Warren, "Behavioural dynamics of intercepting a moving target," *Experimental Brain Research*, vol. 180, no. 2, pp. 303-319, June 2007

[35] G. Diaz, F. Phillips and B. Fajen, "Intercepting moving targets: a little foresight helps a lot," *Experimental Brain Research*, vol. 195, no. 3, pp. 345-360, May 2009

[36] I. Koglbauer, R. Braunstingl and T. Haberkorn, "Modeling human and animal collision avoidance strategies," *Int. Symp. Aviat. Psychol*, pp. 554-559, 2013

[37] T. Haberkorn, I. Koglbauer, R. Braunstingl and B. Prehofer, "Requirements for future collision avoidance systems in visual flight: a human-centered approach," *IEEE Trans. Human-Machine Systems*, vol. 43, no. 6, pp. 583-594, Oct. 2013

[38] C. Chauvin and S. Lardjane, "Decision making and strategies in an interaction situation: collision avoidance at sea," *Transportation Research Part F: Traffic Psychology and Behaviour*, vol. 11, no. 4, pp. 259-269, 2008

[39] Civil Aviation Safety Authority, "CASR Part 91, General operating and flight rules," Civil Aviation

[40] P. Angelov, C. Bocaniala, C. Xydeas, C. Pattchett, D. Ansell, M. Everett, and G. Leng, "A passive approach to autonomous collision detection and avoidance in uninhabited aerial systems," *IEEE Int. Conf. Computer Modelling and Simulation*, pp. 64-69, April 2008

[41] C. Metz, "Basic principles of ROC analysis," *Seminars in Nuclear Medicine*, vol. 8, no. 4, pp. 283-298, Oct. 1978

[42] T. Gandhi,M. Yang, R. Kasturi, O. Camps, L. Coraor and J. McCandless, "Performance characterization of the dynamic programming obstacle detection algorithm," *IEEE Trans. Image Processing*, vol. 15, no. 5, pp. 1202-1214, 2006

[43] J. Lai, J. Ford, L. Mejias, A. Wainwright,P. O'Shea and R.Walker, "Field-of-view, detection range, and false alarm trade-offs in vision-based aircraft detection," *Int. Congress on Aeronautical Sciences (ICAS'12)*, Sep. 2012

[44] J. Kuchar, "Methodology for alerting-system performance evaluation," *AIAA Journal of Guidance, Control, and Dynamics*, vol. 19, no. 2, pp. 438-444, March-April 1996

[45] B. Huska and H. Ferreau and M. Diehl, "ACADO Toolkit - an open source framework for automatic control and dynamic optimization," *Optimal Control Theory and Methods*, vol. 32, no. 3, pp. 298-312, May-June 2011